



HAL
open science

Capillary wave turbulence on a spherical fluid surface in zero gravity

Claudio Falcon, Eric Falcon, Umberto Bortolozzo, Stéphan Fauve

► **To cite this version:**

Claudio Falcon, Eric Falcon, Umberto Bortolozzo, Stéphan Fauve. Capillary wave turbulence on a spherical fluid surface in zero gravity. 2007. hal-00166875v1

HAL Id: hal-00166875

<https://hal.science/hal-00166875v1>

Preprint submitted on 10 Aug 2007 (v1), last revised 9 Feb 2009 (v2)

HAL is a multi-disciplinary open access archive for the deposit and dissemination of scientific research documents, whether they are published or not. The documents may come from teaching and research institutions in France or abroad, or from public or private research centers.

L'archive ouverte pluridisciplinaire **HAL**, est destinée au dépôt et à la diffusion de documents scientifiques de niveau recherche, publiés ou non, émanant des établissements d'enseignement et de recherche français ou étrangers, des laboratoires publics ou privés.

Capillary wave turbulence on a spherical fluid surface in zero gravity

C. Falcón,¹ E. Falcon,^{2,*} U. Bortolozzo,^{1,2} and S. Fauve¹

¹*Laboratoire de Physique Statistique, École Normale Supérieure,
CNRS – 24, rue Lhomond, 75 005 Paris, France*

²*Matière et Systèmes Complexes, Université Paris Diderot–Paris 7,
CNRS – 10 rue A. Domon & L. Duquet, 75 013 Paris, France*

(Dated: August 10, 2007)

We report the observation of capillary wave turbulence on the surface of a fluid layer in low gravity environment. In such conditions, the fluid covers all the internal surface of the spherical container which is submitted to random forcing. The surface wave amplitude displays power-law spectrum over two decades in frequency. This spectrum is found in roughly good agreement with the wave turbulence theory. Such a large band observation has never been reached during ground experiments due to the presence of gravity waves. When the forcing is periodic, two-dimensional spherical patterns are observed on the fluid surface such as subharmonic stripes or hexagons with wavelength satisfying the capillary wave dispersion relation.

PACS numbers: 47.35.Pq, 47.52.+j, 47.54.r, 81.70.Ha

Wave turbulence concerns the study of the dynamical and statistical properties of an ensemble of dispersive waves with nonlinear interactions. Wave turbulence occurs at very different scales in a great variety of systems: surface or internal waves in oceanography [1, 2], Alfvén waves in solar wind [3], plasmas [4], surface waves on elastic plates [5], spin waves in solids. Surprisingly, only a few groups have performed laboratory experiments on this subject so far, exclusively focusing on wave turbulence on fluid surface [6, 7, 8, 9, 10]. These wave turbulence experiments are scarce compared to numerous studies in hydrodynamic turbulence, although various analytical results have been obtained in the framework of wave turbulence or “weak turbulence” theory [11].

Gravity and capillary turbulent wave regimes on a fluid surface are characterised by different Kolmogorov type spectra [10]. These two regimes influence each other and coexist at different scales in the same experiment. Since energy transfers in capillary and gravity regimes are not governed by similar nonlinear processes, it is of primary interest to study pure capillary wave regimes. The importance of the gravity and the capillary effects is quantified by the ratio between the wavelength of the surface wave, λ , and the capillary length, $l_c \equiv \sqrt{\gamma/(\rho g)}$, where γ and ρ are the surface tension and the density of the fluid, respectively, and g is the acceleration of gravity. For usual fluids, l_c is of the order of few mm, corresponding to a critical wavelength $\lambda_c = 2\pi l_c$ of the order of 1 cm. Gravity waves are thus prominent for wavelength larger than few cm. The capillary length cannot be significantly changed using other interfaces between simple fluids and air. It is in an intermediate range between the size of the experiment and the dissipative length. In usual laboratory-scale experiments, this limits both the gravity and capillary regimes to less than a decade in frequency. In a low gravity experiment, one can obtain capillary waves at all wavelengths of the fluid container

of size L , provided that $\lambda_c > L$.

Here, we report the observation of the power spectrum density of the capillary wave turbulence regime over a large range of wavelengths in zero gravity. The invariant-scale power spectrum is found in roughly good agreement with weak turbulence theory. We also study parametric excitation of a fluid in zero gravity by sinusoidally forcing its container. Although the so-called “Faraday instability” has been extensively studied with gravity [12, 13, 14], only one trial has been performed without gravity near the critical point [15]. We report here the first experimental observation of two-dimensional wave patterns on a spherical or cylindrical fluid surface in zero gravity. Applications of this work could be extended to the lattice wrapping on the curved surfaces as well as in condensed matter such as in spherical crystallography [16].

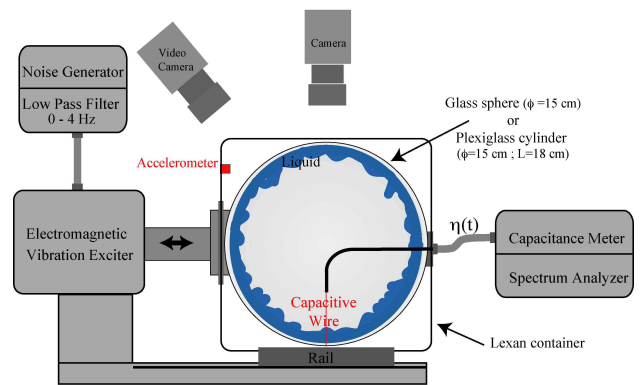


FIG. 1: Sketch of the experimental setup. In microgravity phases, the fluid covers all the internal surface of the container submitted to vibrations.

The experimental setup is sketch in Fig. 1. A container partially filled with a fluid is put down on a rail, and is submitted to vibrations by means of an electromagnetic exciter (BK 4809) via a power amplifier (BK 2706). To

study wave turbulence, the container is driven with a random forcing, supplied by the source of a dynamical analyzer (Agilent 35 670A), and low-pass filtered in the frequency range 0 - 6 Hz by a low pass filter (SR 650). This corresponds to wavelengths of surface waves larger than 1 cm in zero gravity. To study wave patterns, the container is driven with a sinusoidal forcing at frequency f_0 in the range $10 \leq f_0 \leq 70$ Hz, and amplitude of few mm corresponding to a container acceleration of few g . The container geometry is either spherical (15 cm in diameter) or cylindrical (15 cm in diameter, 18 cm in length). Each container is made of a wetting material (Plexiglas cylinder or glass sphere) to avoid that the fluid loses contact with the internal wall of the container during the microgravity phases. According to its geometry, the container is filled with 20 or 30 cl of fluid. This corresponds to an uniform fluid layer of roughly 5 mm depth covering all the internal surface of the container during the microgravity phases. The fluid is either ethanol or water. The local displacement of the fluid is measured with a capacitive wire gauge, 0.1 mm in diameter, plunging into the fluid [10]. This sensor allows wave height measurements from $10 \mu\text{m}$ up to 2 cm with a 0.1 ms response time. A piezoelectric accelerometer (PCB) is screwed on the container to record its acceleration. A dynamical analyzer is used to record the power spectrum of the surface wave amplitude during each microgravity phase. The motion of the fluid surface is visualized with a Nikon camera and recorded with a Sony video camera. Microgravity environment (about $\pm 5 \times 10^{-2}g$) is repetitively achieved by flying with the specially modified *Airbus A300 Zero-G* aircraft through a series of parabolic trajectories which result in zero-gravity periods, each of 20 s.

During microgravity experiments and when no vibration is applied, we observe that the fluid crawls up the sides of the container. The fluid then covers all the internal surface of the tank due to the capillary forces. Contrary to the common sense, no formation of a single sphere of fluid is observed in the middle of the tank, due to these capillary effects. An homogeneous fluid layer is then formed on the internal surface of the tank, confining air in its center. When the container is submitted to a sinusoidal forcing at frequency f_0 , surface wave pattern appears on the fluid surface as shown in Fig. 2 with a cylindrical container. These two-dimensional patterns on the cylindrical fluid surface are either stripes (not shown here) or hexagons (see Fig. 2) depending on the vibrating frequency. By using an other container geometry, one can also observe spherical patterns as shown in Fig. 3.

To understand the mechanism of pattern formation, one records simultaneously the acceleration imposed to the container, and the surface wave height as a function of time. A typical power spectrum density of the container acceleration is shown in the inset of Fig. 4. The main peak at $f_0 = 30$ Hz corresponds to the driving frequency. The typical response of the fluid surface to this excita-

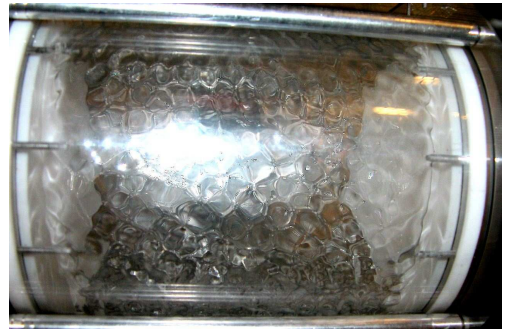


FIG. 2: Two-dimensional cylindrical subharmonic wave patterns (hexagons) under a sinusoidal forcing at frequency $f_0 = 60$ Hz. Cylindrical container filled with 30 cl of ethanol.



FIG. 3: Two-dimensional spherical subharmonic wave patterns under sinusoidal forcing at frequency 60 Hz. Spherical container filled with 20 cl of water.

tion is displayed in Fig. 4. The power spectrum of surface waves shows two main peaks: a subharmonic one close to $f_0/2 \simeq 15$ Hz, and a smaller one at f_0 corresponding to a reminiscence of the driving frequency. The two-dimensional patterns are thus subharmonic ones. The pattern formation can be understood at first sight as simple parametric excitation in zero gravity. However, the patterns are not stationary and their dynamics appears to be very complex: a sloshing motion which depends on the jitters of residual gravity is usually superimposed to the parametric excitation. A complete dynamical description of the pattern deserves further studies.

The pattern wavelength, λ , is then measured as a function of the driving frequency, f_0 . As shown in the inset of Fig. 5, λ is found to decrease with increasing f_0 . Using the dispersion relation of pure capillary waves in the deep layer limit, $\omega^2 = (\gamma/\rho)k^3$ with $k \equiv 2\pi/\lambda$ and $\omega = 2\pi f$ where $f = f_0/2$ is the pattern frequency, one have $k^3 = cf_0^2$ where $c = \pi^2\rho/\gamma$ is a constant depending on the fluid density, ρ , and surface tension, γ . The

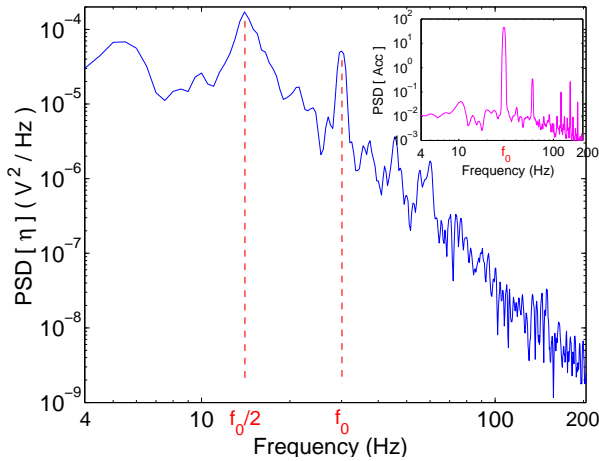


FIG. 4: Typical subharmonic response of patterns in zero-gravity. Power spectrum density of surface wave height. $f_0 = 30$ Hz is the driving frequency. $f_0/2$ is the main response frequency. Inset: Power spectrum density (PSD) of the container acceleration showing the driving frequency f_0 .

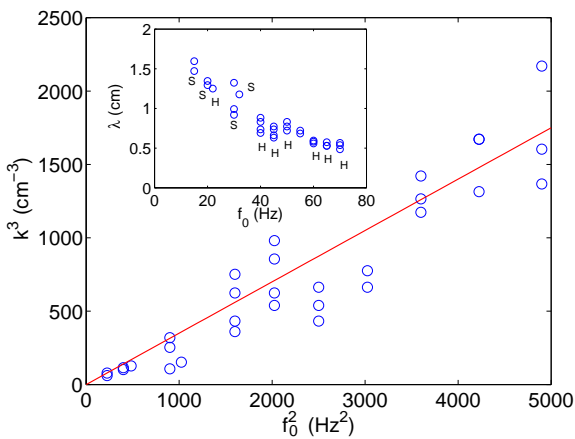


FIG. 5: Pattern wave number cubed, k^3 , as a function of the driving frequency squared, f_0^2 . Solid line of slope $0.35 \text{ s}^2/\text{cm}^3$. Inset: pattern wavelength, λ , as a function of the driving frequency, f_0 . Symbols “S” and “H” correspond to stripe and hexagon patterns respectively. Fluid is ethanol.

pattern wave number cubed, k^3 , is thus plotted in Fig. 5 versus the driving frequency squared, f_0^2 . k^3 is found roughly proportional to f_0^2 with the expected coefficient $c = \pi^2 \rho / \gamma \simeq 0.35 \text{ s}^2/\text{cm}^3$ (extracted from ethanol properties $\rho = 790 \text{ kg/m}^3$; $\gamma = 22 \times 10^{-3} \text{ N/m}$) as shown by the solid line in Fig. 5. The dispersion relation of capillary waves in zero gravity is thus obtained even in the low frequency regime where gravity waves are usually present.

Before showing wave turbulence results in zero-gravity, let us now recall some results in presence of gravity [10]. A square container is filled with a 20 mm ethanol depth. One plunging wave maker is driven with random noise excitation from 0 to 6 Hz. A typical power

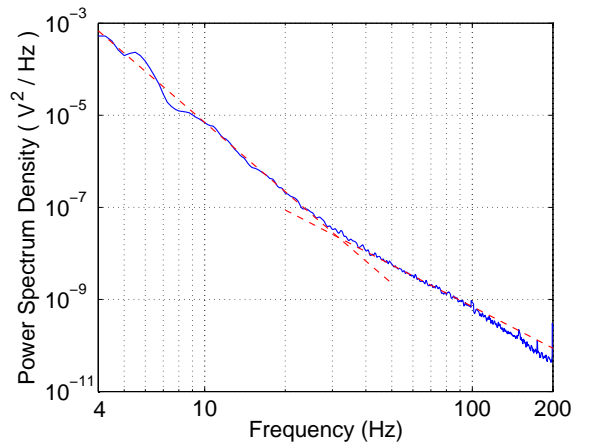


FIG. 6: Power spectrum density of surface wave height *in presence of gravity*. Random forcing 0 - 6 Hz. Slopes of dashed lines are -5 (upper) and -3 (lower) corresponding respectively to gravity and capillary wave turbulence regimes. Rectangular container filled with a 20 mm ethanol depth.

spectrum of the surface wave amplitude in presence of gravity is shown in Fig. 6. The spectrum displays two power laws, and a cross-over is observed near 30 Hz between both regimes. This corresponds to the transition between gravity to capillary wave turbulence [10]. At high frequencies (> 100 Hz), dissipation dominates and ends the energy cascade. The cross-over corresponds to a wave number k of the order of the inverse of the capillary length, that is for a critical frequency, $f_c = \sqrt{g/(2\pi^2 l_c)} \propto g^{3/4}$. The capillary length l_c being of order of few mm for usual fluids, the critical frequency f_c is thus expected of the order 20 Hz in roughly good agreement with the one observed in Fig. 6 (see also Ref. [10]). Such a critical frequency corresponds to a wavelength of the order of 1 cm. When $g \rightarrow 0$, the cross-over frequency between both regimes is then predicted to be pushed away to very low frequency. For our microgravity precision, $\pm 0.05g$, the capillary length then is expected to be close to cm, and the cross-over frequency of the order of 1 Hz, corresponding to wavelength of the order of 10 cm. Thus, in microgravity, for our frequency range (4 Hz up to 500 Hz), the power spectrum of surface wave amplitude should not be polluted by gravity waves.

Let us now present our wave turbulence results in zero gravity. To wit the cylindrical container is submitted to low-frequency random forcing in low-gravity. Surface waves with erratic motions then appears on the free surface as schematically shown in Fig. 1. The power spectrum of surface wave amplitude then is recorded, and is shown in Fig. 7. One single power-law spectrum is observed on two decades in frequency. Whatever the geometry of the tank (sphere or cylinder) and the large scale forcing (random or sinusoidal), the exponent is close to -3 (see Fig. 7). This power-law exponent has roughly

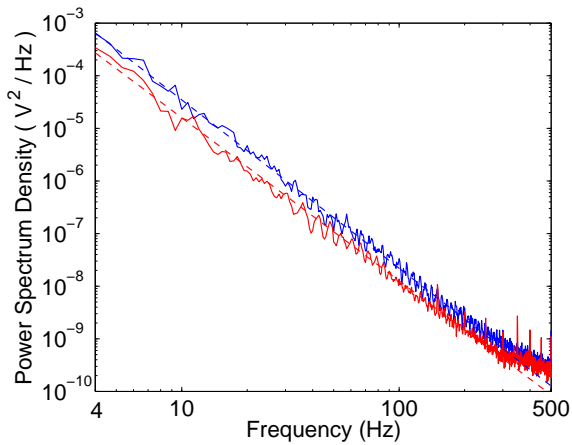


FIG. 7: Power spectrum density of surface wave height *in zero gravity*. Lower curve: Random forcing 0 - 6 Hz. Upper curve: Sinusoidal forcing at 3 Hz. Dashed lines had slopes of -3.1 (lower) and -3.2 (upper). Cylindrical container filled with 30 cl of ethanol.

the same value that the one found under gravity for the capillary wave turbulence regime (see Fig. 6). Weak turbulence theory predicts a $f^{-17/6}$ scaling of the surface height spectrum for the pure capillary regime [17]. This expected $f^{-2.8}$ scaling is close to the f^{-3} one reported here both with or without gravity. Kolmogorov-like spectrum of the capillary wave turbulence regime is thus observed in Fig. 7 over two decades in frequency. To our knowledge, this large range of frequencies has never been reached with ground experiments. This allows to study better the capillary wave turbulence regime. Under gravity, the power spectrum in Fig. 6 is limited at low frequencies (≤ 30 Hz) by gravity waves and at high frequencies (≥ 100 Hz) by a cut-off frequency related to the meniscus diameter on the capacitive wire gauge. In microgravity environment, this latter effect vanishes since the meniscus diameter becomes of the order of the typical size of the container. In microgravity, the power spectrum in Fig. 7 is limited at much higher frequency (~ 400 Hz) due to the low signal-to-noise ratio.

We have reported the observation of capillary wave turbulence on a fluid surface in zero-gravity. When the container is submitted to random forcing, we observe an invariant-scale power spectrum of wave amplitude on two decades in frequency in roughly good agreement with wave turbulence theory. This spectrum is independent on the large-scale forcing parameter. When the container is submitted to periodic forcing, we report the first observation of two-dimensional subharmonic patterns (stripes, hexagons) on a spherical or cylindrical fluid surface. Their wavelengths lead to a measurement of the dispersion relation of linear capillary waves in zero gravity. These patterns results from a simple parametric excitation with no boundary effects. Their dynam-

ical description is much more complex and results from the interaction between two instabilities (sloshing motion and parametric amplification). Understanding their dynamics as well as the pattern selection (role of viscosity, two-frequency periodic forcing...) deserves further studies both experimentally and theoretically.

We greatly acknowledge the help of Y. Garrabos. This work has been supported by the Centre National d'Études Spatiales. The flight has been provided by Novespace. *Airbus A300 Zéro-G* aircraft is a program of CNES. We gratefully acknowledge the Novespace team for his kind technical assistance. C. F. has a fellowship of CONYCIT and U. B. a fellowship of Ville de Paris. This work has been supported by ANR Turbonde BLAN07-3-197846 and by CNES.

* Corresponding author; Email address: eric.falcon@univ-paris-diderot.fr

- [1] Y. Toba, J. Ocean Soc. Jpn. **29**, 209 (1973); K. K. Kahma, J. Phys. Oceanogr. **11**, 1503 (1981); G. Z. Forristall, J. Geophys. Res. **86**, 8075 (1981); M. A. Donelan et al., Philos. Trans. R. Soc. London A **315**, 509 (1985)
- [2] Y. V. Lvov, K. L. Polzin and E. G. Tabak, Phys. Rev. Lett. **92**, 128501 (2004)
- [3] R. Z. Sagdeev, Rev. Mod. Phys. **51**, 1 (1979)
- [4] K. Mizuno and J. S. DeGroot, Phys. Fluids **26**, 608 (1983)
- [5] G. Düring, C. Jossierand and S. Rica, Phys. Rev. Lett. **97**, 025503 (2006)
- [6] W. B. Wright, R. Budakian and S. J. Putterman, Phys. Rev. Lett. **76**, 4528 (1996); W. B. Wright, R. Budakian, D. J. Pine and S. J. Putterman, Science **278**, 1609 (1997)
- [7] M. Lommer and M. T. Levinsen J. Fluoresc. **12**, 45 (2002); E. Henry, P. Alstrøm and M. T. Levinsen, Europhys. Lett. **52**, 27 (2000)
- [8] M. Yu. Brazhnikov, G. V. Kolmakov and A. A. Levchenko, Sov. Phys JETP **95**, 447 (2002); M. Yu. Brazhnikov et al., Europhys. Lett. **58**, 510 (2002); G. V. Kolmakov et al. Phys. Rev. Lett. **93**, 074501 (2004)
- [9] M. Onorato et al. Phys. Rev. E **70**, 067302 (2004)
- [10] E. Falcon, C. Laroche and S. Fauve, Phys. Rev. Lett. **98**, 094503 (2007); E. Falcon, S. Fauve and C. Laroche, Phys. Rev. Lett. **98**, 154501 (2007)
- [11] V. E. Zakharov, V. S L'vov and G. E. Falkovitch, *Kolmogorov Spectra of Turbulence I* (Springer-Verlag, Berlin, 1992)
- [12] M. Faraday, Phil. Trans. R. Soc. London **52**, 299 (1831).
- [13] T. B. Benjamin and F. Ursell, Proc. Roy. Soc Lond. A **225**, 505 (1954).
- [14] W. S. Edwards and S. Fauve, J. Fluid Mech. **278**, 123 (1994), and references therein.
- [15] D. Beysens, R. Wunenburger, C. Chabot and Y. Garrabos, Microgravity Science and Technology **11**, 113 (1998)
- [16] A. R. Bausch et al., Science **299**, 1716 (2003)
- [17] V. E. Zakharov and N. N. Filonenko, J. App. Mech. Tech. Phys. **8**, 37 (1967).